

MHD waves at a spherical interface modelling coronal global EIT waves

M. Douglas and I. Ballai

SP²RC, Department of Applied Mathematics, University of Sheffield, Sheffield S3 7RH, UK
email: mark.douglas;i.ballai@sheffield.ac.uk

Abstract. Energetically eruptive events such as flares and coronal mass ejections (CMEs) are known to generate global waves, propagating over large distances, sometimes comparable to the solar radius. In this contribution EIT waves are modelled as waves propagating at a spherical density interface in the presence of a radially expanding magnetic field. The generation and propagation of EIT waves is studied numerically for coronal parameters. Simple equilibria allow the explanation of the coronal dimming caused by EIT waves as a region of rarified plasma created by a siphon flow.

Keywords. waves, hydrodynamics, Sun: Corona, Sun: oscillations

1. Introduction

It has been known for some time that sudden energy releases (e.g. flares, CMEs, ejectae) can generate large-scale, propagating MHD waves in different layers of the solar atmosphere. One of the most-studied large-scale coronal waves is the *EIT wave*, so-called as they were first observed by the EIT instrument onboard SoHO. EIT waves are often observed as circular fronts propagating away from the site of the associated energy release with speeds of 200–400 km s⁻¹ at an approximately constant altitude (Thompson *et al.* 1999). Given the poor time resolution of the EIT instrument, the nature of EIT waves is still a matter of debate. By analysing TRACE data Ballai *et al.* (2005) showed that EIT waves observed by the EUV instrument exhibit oscillatory behaviour with a period of approximately 400 seconds. In contrast, Attrill *et al.* (2007) illustrated a model where EIT waves are, in fact, a succession of reconnection events.

Another question about EIT waves is the connection of these waves to other global phenomena. Flares are known to generate high-velocity chromospheric waves (Moreton and Ramsey 1960) called Moreton waves propagating with speeds of 1 000–2 000 km s⁻¹, considered to be super-Alfvénic shock waves. Flares also generate MDI waves in the photosphere, with speeds of a few hundred km s⁻¹ (Donea *et al.* 2006). The precise relationship between these waves and flares is an open problem.

In this paper we model EIT waves as MHD surface waves in spherical geometry, a natural extension of studies by, e.g. Wentzel (1979); Parker (1978); Edwin and Roberts (1983). A recent review on theoretical approaches of wave propagation under solar conditions can be found in Nakariakov and Verwichte (2005); De Pontieu and Erdélyi (2006); Erdélyi (2006a,b); Banerjee *et al.* (2007).

2. Governing equation

We assume an isothermal and ideal atmosphere in hydrostatic equilibrium in spherical geometry with constant density. The radially-directed magnetic field takes the form $\mathbf{B}_0 = B_0(r)\hat{\mathbf{e}}_r$, $B_0(r) = A_B/r^2$, where A_B is a constant representing the magnetic flux. Since

the magnetic field is force-free, and there is no gravity, the background pressure must be constant. All perturbations are separable and are expressed as

$$f(r, \theta, \phi, t) = \hat{f}(r)Y_l^m(\theta, \phi) \exp(i\omega t), \quad (2.1)$$

where $Y_l^m(\theta, \phi)$ is the real part of the spherical harmonic and l is the spherical degree. The linearised equations of ideal MHD can be reduced to the fourth order ODE (Douglas and Ballai 2007):

$$\hat{v}_r = \frac{c_0^2}{\omega^2} \frac{d}{dr} \left(\frac{\frac{\omega^2 - \alpha^2}{r^2} \frac{d}{dr} (r^2 \hat{v}_r) + \zeta + \frac{\omega^2 v_A^2}{c_0^2} \frac{d\hat{v}_r}{dr}}{\beta^2 - \omega^2} \right), \quad (2.2)$$

where

$$\alpha^2 = k_r^2 v_A^2, \quad \beta^2 = k_r^2 (c_0^2 + v_A^2), \quad k_r^2 = l(l+1)/r^2, \quad \text{and} \quad \zeta = v_A^2 \frac{d^2}{dr^2} \left(\frac{1}{r^2} \frac{d}{dr} (r^2 \hat{v}_r) \right).$$

3. Particular case: the hydrodynamic limit

Equation (2.2) describes the radial velocity perturbations in spherical geometry with a magnetic field $\propto 1/r^2$. In the particular case of magnetic-free atmosphere the preferential direction of the magnetic field disappears and the propagation of a disturbance becomes homogeneous. In this case, $v_A \rightarrow 0$, so Eq. (2.2) reduces to

$$\hat{v}_r + c_0^2 \frac{d}{dr} \left(\frac{1}{\omega^2 - s_l^2} \frac{1}{r^2} \frac{d}{dr} (r^2 \hat{v}_r) \right) = 0, \quad (3.1)$$

where $s_l^2 = (l(l+1)c_0^2)/r^2$ is the squared Lamb frequency. Eq. (3.1) has been solved by Douglas and Ballai (2007) and the solutions can be expressed in terms of Bessel functions. We can derive the pressure $\hat{p}(r)$ from the expression of $\hat{v}(r)$ by considering the radial momentum equation.

Since our goal is to study the propagation of waves *along* a spherical interface, we consider waves propagating at $r = R_*$; this surface is defined by a density discontinuity, with $\rho_0(r) = \rho_i$ if $r < R_*$ and $\rho_0(r) = \rho_e$ otherwise. The solutions of Eq. (3.1) must satisfy the continuity of radial momentum and of pressure at the interface, together with the requirement of $\hat{v}_r(r)$ being regular at $r = 0$ and evanescent at $r \rightarrow \infty$. These conditions allow us to derive the *dispersion relation for hydrodynamic spherical surface waves at a density discontinuity*

$$\begin{aligned} & \left((\rho_i - \rho_e)(l+1)J_{l+\frac{1}{2}}(X) + \rho_e X J_{l-\frac{1}{2}}(X) \right) \times \\ & \times J_{-\frac{1}{2}-l}(X_e) + J_{l+\frac{1}{2}}(X) \rho_i X_e J_{\frac{1}{2}-l}(X_e) = 0. \end{aligned} \quad (3.2)$$

Here $c_0 = (\gamma p_0/\rho_i)^{\frac{1}{2}}$, $c_e = (\gamma p_0/\rho_e)^{\frac{1}{2}}$, $X = \omega R_*/c_0$, $X_e = \omega R_*/c_e$. In the above expression, $J_k(z)$ is the Bessel function of fractional order k . A simple inspection of the dispersion relation Eq. (3.2) reveals that the effect of spherical geometry is to introduce Bessel functions whose argument and order depend on the spherical degree, l . The dispersion relation is a highly transcendental implicit equation for ω , which has been numerically solved for $l = 0-30$ by Douglas and Ballai (2007)

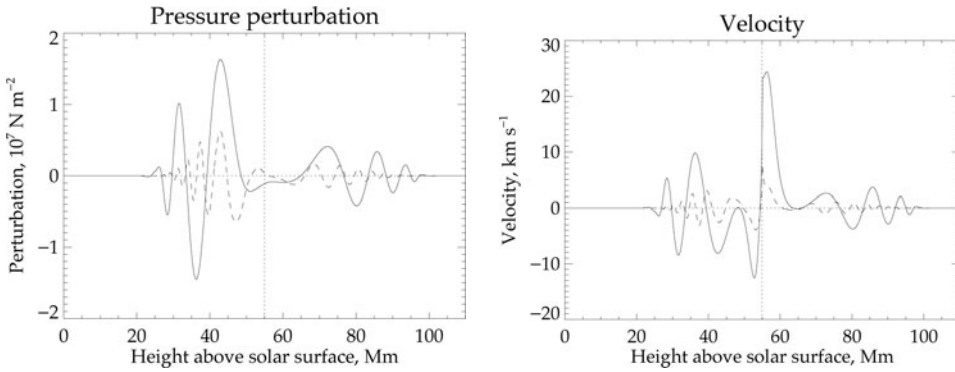


Figure 1. Snapshots of the numerically-calculated spatial solution of Eq. (3.3) for fixed $t = 237$ s and varying r for $l = 500$ (solid line), $l = 1500$ (dashed line) and $\rho_i/\rho_e = 2$. The left-hand plot shows the pressure perturbation, $p(r, t)$, and the right-hand plot shows the velocity perturbation, $v(r, t)$. The horizontal dotted line is the initial undisturbed state and the vertical dotted line represents the location of the initial pressure pulse.

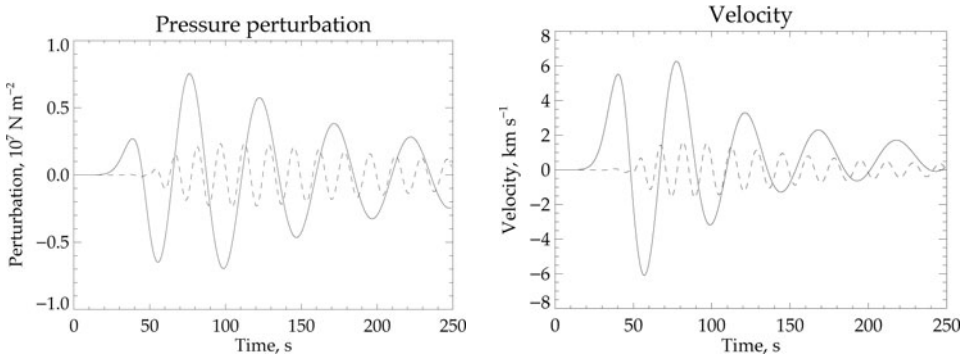


Figure 2. The same as Figure 1, but with r (not t) fixed. r is 8000 km above the interface.

A different view on waves generated by an impulsive source propagating at an interface can be gained by writing the governing equations as the second-order PDE

$$\frac{\partial^2 p}{\partial t^2} - \frac{c_s^2}{r^2} \frac{\partial}{\partial r} \left(r^2 \frac{\partial p}{\partial r} \right) + \frac{c_s^2 l(l+1)}{r^2} p = 0, \quad p(r, 0) = p_0 + p_* \delta(r - R_*). \quad (3.3)$$

In Eq. (3.3) p_0 is the background pressure, p_* is the excess pressure at the location of the impulse, which itself is R_* . This equation is solvable and the solutions are given in terms of spherical Bessel functions. Using an explicit finite-difference scheme the variation of pressure perturbation and radial velocity are shown in Figures 1 and 2 for different values of l and a density ratio $\rho_i/\rho_e = 2$.

Figure 1 illustrates the dependence of the pressure perturbation and radial velocity amplitude with radial distance at $t = 237$ s. The temporal change in the amplitudes of these quantities are shown in Figure 2 at a fixed radial distance $r = 8000$ km above the interface (which is itself located at $1.08 R_\odot$). In Figure 1 we observe the asymmetric distribution of pressure in the two domains, the pressure beneath the interface being almost 6 times higher. This pressure difference must generate a very strong radial pressure gradient, driving a siphon flow which can lift up material from below to higher altitudes. Projected to the case of a CME, this result implies that the largest part of the material expelled by a CME comes from the cooler regions below the CME.

The second important conclusion of Figure 1 is that the oscillatory behaviour of waves starts some distance away from the initial pulse; for the quantities used here oscillations start only after approximately 10 000 km, depending on l . According to these results the first stage of a spherical wave consists of a strong shock which decays after some distance and wave-like motion starts to appear. It is most probable that the oscillatory behaviour of EIT waves found by Ballai *et al.* (2005) is related to this stage of EIT wave evolution. The temporal variation of the pressure and radial velocity shows a decaying pattern as the signal travels away from the source due to geometrical dissipation. We can also comment on the effect of changing the harmonic degree l ; it appears that waves of lower degree travel faster, and that waves of lower degree have far fewer visible wavecrests.

4. Conclusions

Here we have modelled EIT waves as surface waves propagating along a spherical density interface at a constant radius. The highly transcendental dispersion relation for such waves in a field-free atmosphere is derived.

The results of numerical simulations of radial surface waves, generated by a sudden, large pressure pulse excitation, are presented. It was shown that the propagation of these waves either side of the interface is asymmetric, leading to a large pressure gradient across the interface. The oscillatory behaviour of these waves is found not to start until quite some distance away from the impulsive source, and the amplitude of these oscillations exhibits damping. Thus, the dimming seen in observations of EIT waves is explained as evidence of a region of rarified plasma, where the large pressure gradient has evacuated much of the material away.

The present investigation will be extended in the future to include a full magnetic case, which we expect to exhibit much more complex behaviour, and the effects of a finite spherical shell. We also aim to show that MHD waves can be trapped in the low corona.

Acknowledgements

M. D. is grateful to STFC for financial support. I. B. acknowledges the financial support by The Royal Society, The National University Research Council, Romania (CNCSIS-PN-II/531/2007) and NFS Hungary (OTKA, K67746).

References

- Attrill, G. D. R., Harra, L. K., van Driel-Gesztelyi, L. *et al.* 2007, *Astron. Nachr.* 328, 760
 Ballai, I., Erdélyi, R. and Pintér, B. 2005, *ApJ* (Letters) 633, L145
 Banerjee, D., Erdélyi, R., Oliver, R. and O'Shea, E. 2007, *Solar Phys.* 246, 3
 De Pontieu, B. and Erdélyi, R. 2006, *Phil. Trans. Roy. Soc. A* 364, 383
 Donea, A.-C., Besliu-Ionescu, D., Cally, P. S. *et al.* 2006, *Solar Phys.* 239, 113
 Douglas, M. and Ballai, I. 2007, *Astron. Nachr.* 328, 769
 Edwin, P. M. and Roberts, B. 1983, *Solar Phys.* 88, 179
 Erdélyi, R. 2006a, *Phil. Trans. Roy. Soc. A* 364, 351
 Erdélyi, R. 2006b, in Fletcher, L. and Thompson, M. (eds) *SOHO 18/GONG 2006/HELAS I: Beyond the spherical Sun*, Sheffield, ESA SP-624, 15.1
 Moreton, G. E. and Ramsey, H. E. 1960, *PASP* 72, 357
 Nakariakov, V. M. and Verwichte, E. 2005, *LRSP* 2, 3
 Parker, E. N. 1978, *ApJ* 221, 368
 Thompson, B. J., Gurman, J. B., Neupert, W. M. *et al.* 1999, *ApJ* (Letters) 517, L151
 Wentzel, D. G. 1979, *ApJ* 227, 319